Arabian Journal of Chemistry 16 (2023) 105229

Contents lists available at ScienceDirect

Arabian Journal of Chemistry

journal homepage: www.sciencedirect.com

Original article

Core-shell iron oxide-platinium@metal organic framework/epirubicin nanospheres: Synthesis, characterization and anti-breast cancer activity

Jiadi Li [a], Yuxin Zhou [a], Shuixin Yan [a], Weizhu Wu [a,*], Majid Sharifi [b]

[a] Department of Breast Surgery, The Affiliated Lihuili Hospital of Ningbo University, Ningbo 315040, China
[b] Department of Nanotechnology, Faculty of Advanced Sciences and Technology, Tehran Medical Sciences, Islamic Azad University, Tehran, Iran

ARTICLE INFO

Article history:
Received 20 June 2023
Accepted 31 August 2023
Available online 4 September 2023

Keywords:
Breast cancer
Metal-Organic Frameworks
Photodynamic
Chemotherapy
Epirubicin

ABSTRACT

Potential cancer therapy can be accomplished by utilizing nano-based platforms that supply facilitated drug penetration inside cancer cells. In this paper, an intelligent therapeutic nano-based system derived from metal–organic framework (MOF) core–shell hybrids with the capacity of potential drug loading, tumor microenvironment-triggered drug release as well as promising cell penetration was developed. The core–shell iron oxide-platinium@MOF/epirubicin (Fe_3O_4-Pt@MOF/EPI) nanospheres were constructed, where these nanoplatforms endow the system with the capability of pH-responsive drug release. The synthesized Fe_3O_4-Pt@MOF/EPI nanoparticles were characterized using different well-known techniques. The Fe_3O_4-Pt@MOF/EPI nanospheres were shown to have a dried size of around 50 nm (evidenced by SEM analysis), a spherical/core–shell/porous structure (evidenced by TEM), and an average hydrodynamic size of 92.89 nm (evidenced by DLS). Additionally, TGA analysis revealed that Fe_3O_4-Pt@MOF/EPI nanospheres had a weight loss at temperatures between 220 and 450 °C associated with the removal of MOF and EPI from the structure of core–shell nanospheres. The N_2 adsorption–desorption data also reflected the porosity of core–shell Fe_3O_4-Pt@MOF nanospheres by indicating type IV behavior with an apparent hysteresis loop in the range of 0.38–0.98. Furthermore, XRD analysis disclosed the changes in the peak intensity at positions of 57.2° and 39.5°, which indicated the effects of loaded MOF on Fe_3O_4-Pt nanosphere. Moreover, core–shell Fe_3O_4-Pt@MOF/EPI nanospheres showed high loading capacity and drug release in a pH-responsive manner. Cell viability and cellular uptake assays on mouse fibroblast (NIH3T3) and triple-negative 4 T1 breast (TNFB) tumors showed that the core–shell Fe_3O_4-Pt@MOF/EPI nanospheres effectively inhibited TNFB cancer cells proliferation through inducing higher cell penetration compared to free EPI while having good biocompatibility against NIH3T3 cells. In conclusion, the present study may provide useful information about the development of efficient anticancer platforms against breast cancer cells, while further *in vivo* and pre-clinical assays are required to support this study.

1. Introduction

Triple-negative 4TI breast (TNFB) tumor, a subset of breast cancer, is one of the most aggressive malignancies with a high mortality rate of over 70%, defined by the lack of expression of estrogen, progesterone and HER2 receptors (da Silva, Nunes et al. 2020). Due to the high likelihood of recurrence, high drug resistance, high potential for metastasis, and poor prognosis of TNFB tumors, current treatments, including chemotherapy and surgery, have not been very effective in killing this kind of cancer cells (Marra, Trapani et al. 2020). Therefore, TNFB tumor therapy requires the application of new technologies, such as drug delivery using the nano-platform, which can assist in effective combination therapies (Sharifi, Hosseinali et al. 2019, Jain, Kumar et al. 2020). In this regard, the use of metal nanospheres, particularly iron oxide (Fe_3O_4) with various coatings due to several advantages, including ideal biocompatibility, high loading capacity, imaging capability, multimodal cancer treatment, controlled catalytic activities, as well as targeting and feasible production, has received great attention, recently (Sharifi, Hasan et al. 2020, Sharifi, Jafari et al. 2020,

* Corresponding author.
E-mail address: 13957402451@163.com (W. Wu).

Peer review under responsibility of King Saud University.

Production and hosting by Elsevier

https://doi.org/10.1016/j.arabjc.2023.105229
1878-5352/

DİNÇER, GETİREN et al. 2021, Khan, Sharifi et al. 2021, Klein, Otto et al. 2021, Zhao, Li et al. 2021). However, Fe_3O_4 nanoparticles are faced with some challenges such as limited drug loading, probable side effects at high concentrations, slow degradation rate with high agglomeration potency, and retention in vital organs. According to several studies, adding metal–organic frameworks (MOF) coatings on metal nanospheres to develop core–shell nanostructures increases the porosity and functionality while also allowing for regulated drug release in an acidic environment (Bag, Wang et al. 2016, Yang, Xia et al. 2017, Wu, Gao et al. 2018, Wang, Yu et al. 2020, Cui, Zhao et al. 2021, Falahati, Sharifi et al. 2022). Additionally, MOF coating as a shell on the core materials improves the nanospheres' biocompatibility, catalytic activity, and colloidal stability (Wang, DeKrafft et al. 2012, Meng, Zhang et al. 2018, Chen, Zhang et al. 2019, Qi, Ye et al. 2020, Yue, Cao et al. 2021, Yang, Zeng et al. 2022). In this regard, in addition to increasing drug stability and permeability in Hela and triple-negative MDA-MB-231 cancer cells, Chowdhuri, Bhattacharya et al. (2016) and Alijani, Noori et al. (2020) were able to demonstrate good biocompatibility in NIH3T3 and HUVEC normal cells using Fe_3O_4@IRMOF-3/folic acid and Fe_3O_4@MOF-doxorubicin-carbon-aptamer, respectively. By combining chemotherapy with hyperthermia to increase the drug permeability and controlled release of doxorubicin, Chen, Liu et al. (2019) also demonstrated that the Fe_3O_4@poly[dopamine]@ZIF-90/doxorubicin inhibited the proliferation and development of Hela cancer cells more effectively than the free drug. In a mouse model, Xiang, Qi et al. (2020) revealed that Fe_3O_4@C-poly[vinylpyrrolidone]@doxorubicin, in comparison to free doxorubicin, reduced efficiently CAL27 tumor size mediated by controlled pH-sensitive drug release, increased biocompatibility and reduced drug toxicity in the main off-target organs.

On the other hand, the history of platinum (Pt) application in the development of anticancer agents began in 1978 (Rottenberg, Disler et al. 2021). Then a wide number of Pt-based derivatives have been developed and assessed as potential anticancer agents. The mechanisms of action of these drugs are associated with DNA interaction and corresponding DNA synthesis impairing (Desoize and Madoulet 2002).

The anticancer drug epirubicin (EPI) is a doxorubicin epimer with a 4′-hydroxyl group inversion on sugar (Plosker and Faulds 1993). The primary mechanism of EPI action is expressed by DNA or RNA damage caused by suppression of topoisomerase II activity, free radical production, downregulation of protein synthesis, and disruption of the cell membrane which finally results in cell cycle arrest (Khasraw, Bell et al. 2012). EPI is less likely to be harmful than doxorubicin, despite the fact that various side effects such as myelotoxic, non-hematological toxicities, and cardiac toxicity have been recorded (Yamaguchi, Fujii et al. 2015). To boost the drug's effectiveness, however, the dose of EPI must be increased for long-term usage, which sharply raises cardiac toxicity (Fogarassy, Vathy-Fogarassy et al. 2019). However, the efficacy of EPI in treating neuroblastoma, liver, lung, stomach, colorectal, squamous cell, cervix, bladder, and ovarian cancers recommends the use of this drug following the development of anticancer platforms. It appears that a nanoplatform can be employed to lessen toxicity issues and increase the efficacy of EPI in cancer treatment. Recently, De Vita, Liverani et al. (2021) demonstrated that using lipid nanovesicles carrying EPI not only successfully inhibits the growth of triple-negative breast cancer cells but also increases the biocompatibility of nanoparticles, which reduces the degree of EPI toxicity. However, the dose and duration of EPI use, drug loading and release levels, and EPI permeability in cancer cells are still some challenges that need to be addressed properly (Jalalian et al., 2018, Chen, Han et al. 2019, Fathian kolahkaj, Derakhshandeh et al. 2019, Tang, Chen et al. 2020, Leng, Li et al. 2021).

Therefore, to treat breast cancer, we present in this study a smart porous core–shell Fe_3O_4-Pt@MOF/EPI nanosphere as an emerging therapeutic modality. In the first step, the nanospheres were synthesized, followed by characterization by different techniques. Afterward, the anticancer effect of porous core–shell Fe_3O_4-Pt@MOF/EPI nanospheres on inhibition of the proliferation of triple-negative 4 T1 breast (TNFB) cells was assessed, while mouse fibroblast cells (NIH3T3) were used as a model of non-cancerous cells. Also, cell penetration analysis was done to assess the drug penetration inside the cells.

2. Material and methods

2.1. Materials

Epirubicin (EPI) and Cell Counting Kit-8 (CCK-8) were obtained from the Sigma Co. (Saint Louis, MO, USA). Dulbecco's Modified Eagle Medium (DMEM) and fetal bovine serum (FBS) were purchased from Thermo Fisher Scientific (Waltham, MA, USA). All other materials were of analytical grade, obtained from Merck Co. (Darmstadt, Germany) and used without further purification.

2.2. Synthesis of Fe_3O_4 nanospheres and core–shell Fe_3O_4-Pt@MOF/EPI nanospheres

To fabricate Fe_3O_4 nanospheres, the modified method of Sharifi, Hasan et al. (2020) was used. In 20 mL of equal parts ethylene glycol and diethylene glycol, 1.62 g of iron chloride, 4.5 g of sodium acrylate, and 4.5 g of sodium acetate were added. The obtained homogeneous solution was heated in a Teflon-lined stainless-steel autoclave at 220 °C. After 10 h, the autoclave was cooled and the Fe_3O_4@poly(acrylamide) nanospheres were separated and washed with ethanol and water, followed by sample drying in vacuum for 24 h. To develop a silicon coating on the nanospheres, 5 mL of aqueous Fe_3O_4@poly(acrylamide) solution was diluted with water and ethanol [1/60 (v/v)]. After sonication of the samples for 40 min, 2 mL of ammonia solution was added to the sample solution. Following the injection of 0.2 mL of tetraethyl-orthosilicate solution dissolved in 10 mL of ethanol into the samples after 30 min, the final product was magnetically collected after 120 min. The Fe_3O_4@poly(acrylamide)@SiO_2 were washed several times with ethanol and water before being vacuum dried for 24 h. The Fe_3O_4@poly(acrylamide)@SiO_2 samples were then heated in an electric oven for 5 h at 650 °C. After cooling at 23 °C, Fe_3O_4@SiO_2 produced in 0.5 M NaOH was mechanically shaken for 7 h to remove SiO_2. Finally, the Fe_3O_4 nanospheres were collected magnetically and repeatedly washed with distilled water and ethanol.

To produce Fe_3O_4-Pt nanosphere, chloroplatinic acid hexahydrate (H_2PtCl_6-$6H_2O$, 0.1 g) and tri-sodium citrate dihydrate ($HOC(COONa)(CH_2COONa)_2{\cdot}2H_2O$, 0.0075 g) were mixed in 500 mL of distilled water under a magnetic stirrer (800 rpm). Then, 25 mL of 0.01 M NaBH4 solution was added to the platinum precursor solution. Finally, 300 mg of Fe_3O_4 nanoparticles in 30 mL of distilled water were added to the above solution and sonicated for 20 min. The resulting particles were then collected by an external magnetic field and washed several times with distilled water.

At the end, zirconium chloride (0.55 g) and terephthalic acid (0.45 g) were added to a solution containing 10 mL of ethanol and 50 mL of N, N-dimethylformamide, under continuous stirring. Following this, a certain quantity of Fe_3O_4-Pt nanospheres (500 mg) were dissolved in 15 mL of ethanol and added to the aforementioned mixture, where they were agitated for 5 min. Finally, the suspension was autoclaved for 12 h at 150 °C. The com-

pleted product was cooled, and then cleaned three times with ethanol and water before being dried at 80 °C.

A specific number of nanocarriers were kept at a predefined concentration of EPI at pH 8.0 for 24 h to load EPI onto the core–shell Fe_3O_4-Pt@MOF nanospheres (at room temperature). Core-shell Fe_3O_4-Pt@MOF/EPI nanospheres were then collected using a magnet, and the samples were repeatedly washed in PBS to remove surface debris and extra EPI from the nanocarriers' surfaces.

2.3. Core-shell Fe_3O_4-Pt@MOF/EPI nanosphere characterization

Scanning electron microscopy (SEM, MIRA3 TESCAN) was used to examine the morphology and size of Fe_3O_4-Pt@MOF/EPI nanospheres. The core–shell, as well as porosity structure of nanospheres, were examined by TEM (JEM – 7100F). Thermogravimetric analysis (TGA) of the samples was evaluated using a thermogravimetric analyzer (TG209-F3, USA) under argon with a heating rate of 10 °C/min in the 20–550 °C range. Also, Zetasizer Nano ZS90 (Malvern Instruments, UK) was used to determine the hydrodynamic size distribution and zeta potential. Additionally, the N2 adsorption analysis was used at 77 K using the Micromeritics ASAP analyzer to study the surface gaps of the nanospheres. To explore the crystalline structure of the samples, the X-ray diffraction pattern (XRD) analysis was performed using a Bruker Advance-D8 equipped with CuKα as irradiation source (λ = 1. 54178 Å).

2.4. Drug loading and release

To measure the EPI loading in core–shell Fe_3O_4-Pt@MOF nanospheres, 250 g nanocomposite was added to EPI solutions with concentrations ranging from 100 to 500 g/mL under constant shaking for 24 h. Then, core–shell Fe_3O_4-Pt@MOF/EPI nanospheres were magnetically separated and washed with a phosphate buffer to remove unbonded EPI from the nanocomposite surface. Next, UV–visible spectroscopy (UV-1800, Shimadzu, Japan) was used to measure the amount of EPI loaded at 482 nm. Finally, EPI loading on the core–shell Fe_3O_4-Pt@MOF/EPI nanospheres was calculated using Equation (1):

$$\begin{aligned} EPI\ loading(\%) = [&(Total\ amount\ of\ EPI\ in initial\ solution \\ &- Amount\ of\ EPI\ remaining\ in\ solution) \\ &/ Amount\ of\ EPI\ remaining\ in\ solution] \times 100 \end{aligned} \quad (1)$$

The dialysis bag method was used to assess the release profile of EPI. This was accomplished by placing 250 g of core–shell Fe_3O_4-Pt@MOF/EPI nanospheres into dialysis bags (MWCO 12000), which were then suspended in 50 mL of PBS solution at various pH values of 6 and 7.5. The solution was shaken continuously at 37 °C and at different time intervals, such as 0.01, 0.25, 0.50, 1, 1.5, 3, 6, 9, 12, 16 and 24 h, 5 mL of solution was withdrawn for further analyses and the same volume of initial buffer was reintroduced to the tank to assure about the sink condition. The amount of EPI release was then measured by UV spectroscopy at 482 nm according to the Equation (2):

$$\text{Cumulative drug release}\,(\%) = \frac{5 \times \sum_{i-1}^{n-1} C_i + 50 \times C_n}{\text{weight of EPI on Fe3O4} - \text{Pt@MOF/EPI core} - \text{shell}} \times 100 \quad (2)$$

C_i and C_n refer to the of EPI concentration at time i and n, respectively.

2.5. In-vitro trials

Triple-negative 4 T1 breast (TNFB) cells and mouse fibroblast cells (NIH3T3) were seeded in flasks by using Dulbecco's modified Eagle's medium (DMEM) and 10% fetal bovine serum along with a 1% penicillin–streptomycin solution. The samples were then incubated with 5% CO_2 and 95% humidity at 37 °C.

2.5.1. Cellular viability and toxicity

To evaluate the cell viability and cytotoxicity of samples on NIH3T3 and TNFB cancer cells after 24 h, WST-8 staining reaction method (tetrazolium salt) with cell count kit-8 (CCK-8) was used. After seeding, 10,000 NIH3T3 and TNFB cancer cells were incubated for 24 h in 96 plates. The cultured samples were then treated with EPI (7.5, 15, 22.5 and 30 μg/mL, based on the report of Moammeri, Abbaspour et al. (2022)), core–shell Fe_3O_4-Pt@MOF nanospheres (15, 30, 45 and 60 μg/mL), or core–shell Fe_3O_4-Pt@MOF/EPI nanospheres (15, 30, 45 and 60 μg/mL). Then, 15 μL of 0.5 mg/mL CCK-8 solution was added to the cells and incubated for 2 h in the dark at 37 °C. Ultimately, the optical density of the cells was read at 450 nm using an ELISA plate reader (Synergy HT Multi-Mode Microplate Reader, BioTek, USA). The survival rate of cells was analyzed using Equation (3).

$$\begin{aligned} Cell\ viability(\%) = [&(Opticaldensityofdosingcells - Optical\ density\ of\ blank) \\ &\div (Opticaldensityofcontrol - Optical\ density\ of\ blank)] \times 100 \end{aligned} \quad (3)$$

2.5.2. Drug or nanocomposite penetration

TNFB cancer cells were seeded in 96-well plates with a density of 1×10^4 cells. TNFB cancer cells were then treated with 22.5 μg/mL EPI and 45 μg/mL nanospheres and incubated for 12 h. After removing the medium, the TNFB cancer cells were washed three times with cold PBS to remove the drug and nanospheres in the culture medium. Finally, the fluorescence intensity of the TNFB cancer cells was read using a fluorometer (Perkin Elmer 3B, Wellesley, MA, USA) with excitation of 482 nm and emission of 590 nm.

2.6. Statistical analysis

All analyses were performed with SPSS 19.0 software (SPSS Inc.). Data were reported as mean ± STD from three experiments. Statistical comparisons were done using one-way / two-way analysis of variance (ANOVA) at levels of $P < 0.05$, $P < 0.01$ and $P < 0.001$.

3. Results and discussion

3.1. Morphological and structural properties

The synthesis of core–shell Fe_3O_4-Pt@MOF/EPI nanospheres was assessed by SEM analysis. Fig. 1A depicts some cracks on the surface of Fe_3O_4-Pt@MOF/EPI nanospheres. As shown in the SEM images (Fig. 1A), the mean size of the core–shell Fe_3O_4-Pt@MOF/EPI nanospheres was around 50 nm. Also, appearance of noticeable Pt signal in the corresponding EDX spectrum (Fig. 1B) allows us to suggest that bimetallic Fe_3O_4-Pt nanoparticles are formed. TEM imaging (Fig. 1C) also demonstrated the formation of core–shell and porous structures.

The DLS data in Fig. 2A provides further information regarding the colloidal stability of synthesized nanospheres. It was shown that the average hydrodynamic size of Fe_3O_4-Pt nanospheres is 79.88 nm and that when MOF and EPI are present, the average particle size increases to 92.89 nm. Therefore, the DLS results showed the suitable size distribution of prepared nanospheres. Also, the

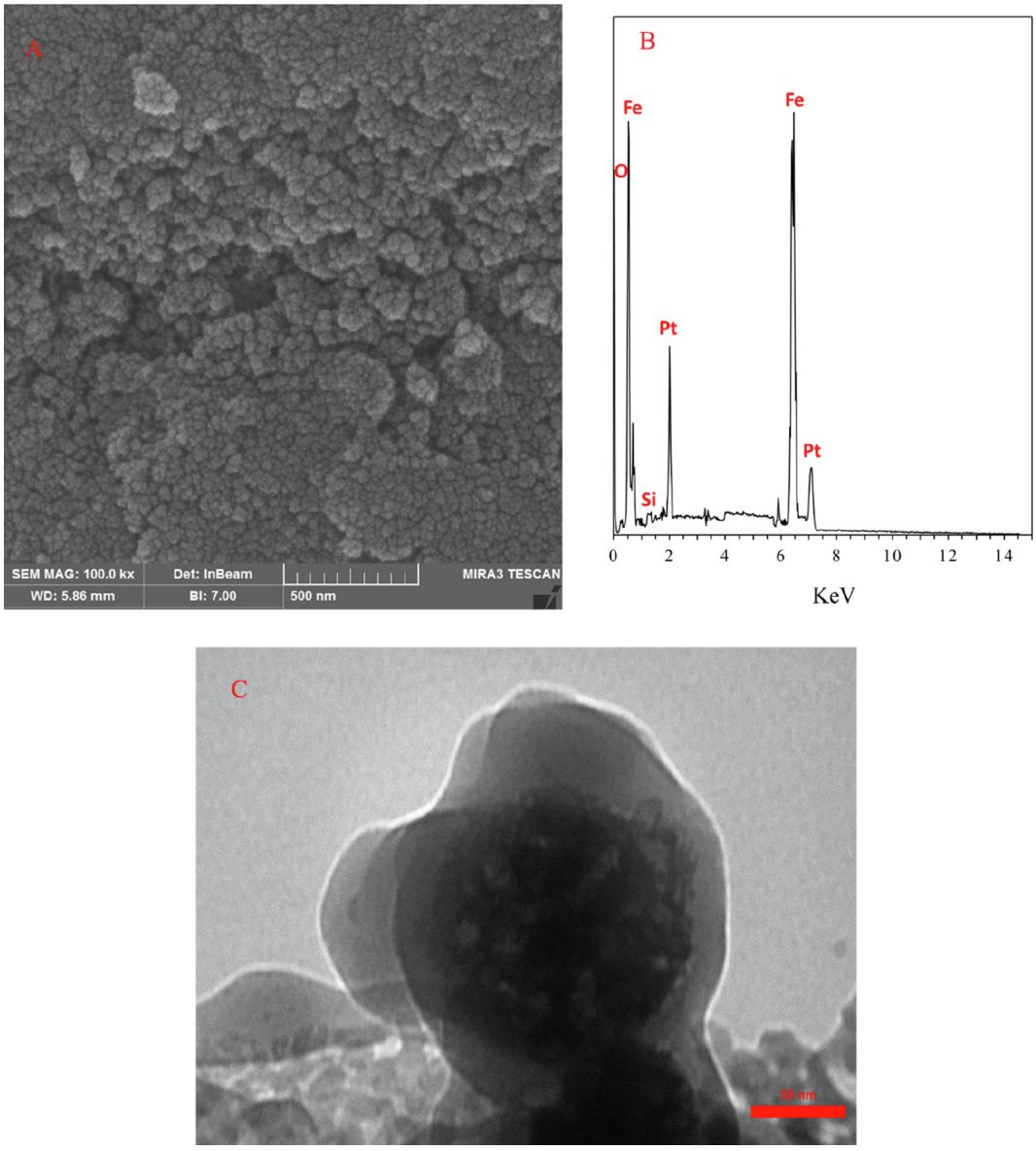

Fig. 1. (A) The SEM image, (B) EDAX spectrum and (C) TEM image of core–shell Fe_3O_4-Pt@MOF/EPI nanospheres.

thermal behavior of the nanospheres in Fig. 2B exhibits that the weight loss of the core–shell Fe_3O_4-Pt nanospheres at temperatures between 150 and 550 °C is related to the removal of solvents from the nanosphere surface. While the weight loss at temperatures between 220 and 450 °C in Fe_3O_4-Pt@MOF and Fe_3O_4-Pt@MOF/EPI is related to the removal of MOF and EPI from the structure of core–shell nanospheres, respectively. This finding indicates the successful loading of MOF and EPI on the Fe_3O_4-Pt nanosphere.

The zeta potential values in Fig. 2C indicate that core–shell Fe_3O_4-Pt@MOF nanospheres had zeta potentials of 16.1 mV, −5.2 mV, −10.3 mV and −18.8 mV, at different pHs of 3, 5, 7 and 9, respectively. However, following EPI loading zeta potential values changed to 21.5 mV, −11.1 mV, −21.9 mV and −29.9 mV, respectively. High and negative zeta potential values confirmed that the core–shell Fe_3O_4-Pt@MOF/EPI nanospheres are resistant to intrinsic aggregation through van der Waals interactions. On the other hand, a negative charge of the core–shell Fe_3O_4-Pt@MOF nanospheres in a range of pH 5-–9 can increase the drug loading by increasing the electrostatic interactions between the core–shell Fe_3O_4-Pt@MOF nanospheres and EPI with a positive charge. The N_2 adsorption–desorption output in Fig. 2D further validates the porosity in the core–shell Fe_3O_4-Pt@MOF nanospheres by indicating type IV behavior with an apparent hysteresis loop in the range of 0.38–0.98. The remarkable capacity of core–shell Fe_3O_4-Pt@MOF nanospheres to improve loading EPI is demonstrated by BET results with a surface of 159.5 m^2/g and cavities with dimensions of 1 and 5.8 nm (a space of 0.26 cm^3/g).

Additionally, the XRD pattern of Fe_3O_4-Pt nanospheres in Fig. 2E shows nine peaks centered at 29.9°, 35.4°, 39.5°, 42.9°, 44.1°, 54.4°, 57.2°, 62.9°, and 68.0°, which correspond to the reflection plane indices of (220), (311), (111), (400), (200), (422), (511), (440) and (220). These results demonstrate the presence of the crystalline cubic phase and the exclusion of any contamination. Additionally, the XRD pattern of core–shell Fe_3O_4-Pt@MOF nanospheres showed that the positioning of the peaks on the Fe_3O_4-Pt nanospheres did not change significantly with the loading of MOF except at 42.9° and 44.1°. Meanwhile, the changes of the

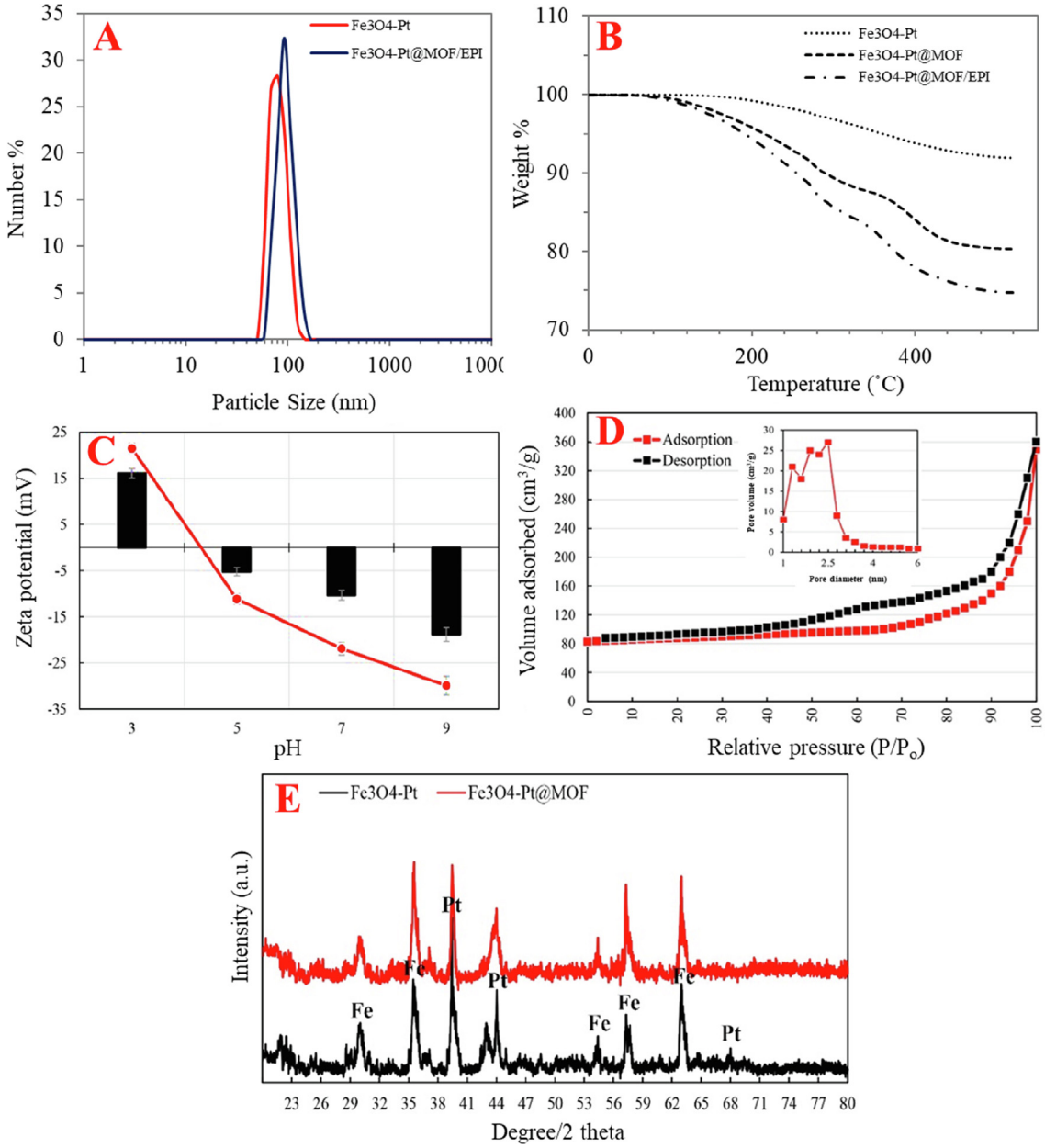

Fig. 2. (A) DLS size distribution of Fe_3O_4 and core–shell Fe_3O_4-Pt@MOF/EPI nanospheres, (B) TGA curves of Fe_3O_4, core–shell Fe_3O_4-Pt@MOF nanospheres and core–shell Fe_3O_4-Pt@MOF/EPI nanospheres, (C) Zeta potentials of core–shell Fe_3O_4-Pt@MOF nanospheres and core–shell Fe_3O_4-Pt@MOF/EPI nanospheres measured in different pH, and (D) N_2 sorption–desorption isotherms of the as-prepared core–shell Fe_3O_4-Pt@MOF nanospheres. The inset exhibits corresponding pore size distribution analysis obtained using the density functional theory. (E) XRD patterns of prepared Fe_3O_4-Pt and core–shell Fe_3O_4-Pt@MOF nanospheres.

peak intensity at positions of 57.2° and 39.5°, indicate the effects of loaded MOF on Fe_3O_4-Pt nanosphere XRD pattern. Overall, the XRD data demonstrate that the crystalline structure of the Fe_3O_4-Pt core does not change significantly when MOF is grown on the Fe_3O_4-Pt platform.

The SEM, DLS, TGA, and XRD analyses revealed the potential loading of the drug on the Fe_3O_4-Pt@MOF nanospheres. However, similar to the results of Ke, Qiu et al. (2012), Chen, Liu et al. (2019) and Chen, Zhang et al. (2019) controlling the amount of MOF loading to prevent asymmetric development was a major challenge of this study. The results of TGA analysis, on the other hand, show an improvement in drug loading efficiency, which is consistent with the findings of Xiang, Qi et al. (2020) and Pooresmaeil, Asl et al. (2021).

3.2. Drug loading and pH-sensitive drug release

As shown in Fig. 3A, increasing EPI concentration increases drug loading while maintaining the core–shell Fe_3O_4-Pt@MOF concentration constant. However, as EPI concentration increases, the percentage of EPI loading efficiency decreases. Fig. 3A output shows the highest percentage of EPI loading at a concentration of 100 g/mL, with 84.1% loading. According to the profile presented, the highest EPI loading in core–shell Fe_3O_4-Pt@MOF nanospheres is at 200 g/mL with an efficiency of 81.2 %.

Fig. 3B depicts EPI release from core-shell Fe_3O_4-Pt@MOF/EPI nanospheres, revealing that EPI release has a time-dependent profile. EPI release rates at pH 7.4 and 6 are generally rapid in the first 3 h and then decrease over time. Rapid drug release may be due to

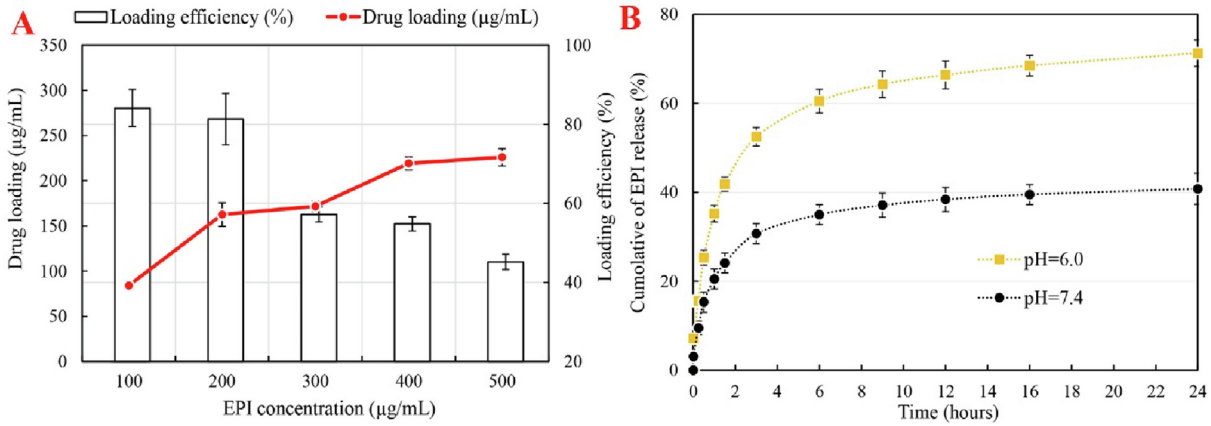

Fig. 3. (A) EPI loading and efficiency percentage, and (B) Quantitative analyses of EPI diffusion at 37 °C at pH 6 and pH 7.4.

surface EPI in the early stages, and slow release may be due to an EPI release inside the core–shell Fe_3O_4-Pt@MOF/EPI nanospheres. Even though changing the pH from 7.4 to 6 increases EPI release, the relevant output in Fig. 3B shows that the burst release in pH 6, is greater than in pH 7.4. This parameter represents that core–shell Fe_3O_4-Pt@MOF/EPI nanospheres act as a pH-sensitive platform for EPI release. The initial burst release rate in 30 min was 25.3 % at pH 6 and 15.3 % at pH 7.4. Overall, the developed nanospheres appear to be capable of performing pH-sensitive drug release in a tumor microenvironment.

The increased loading level and drug release rate can be attributed to an increase in the abundance and size of the cavities created on the nanospheres as a result of the loading of MOF on the core–shell Fe_3O_4-Pt nanospheres. According to Rao, Chen et al.

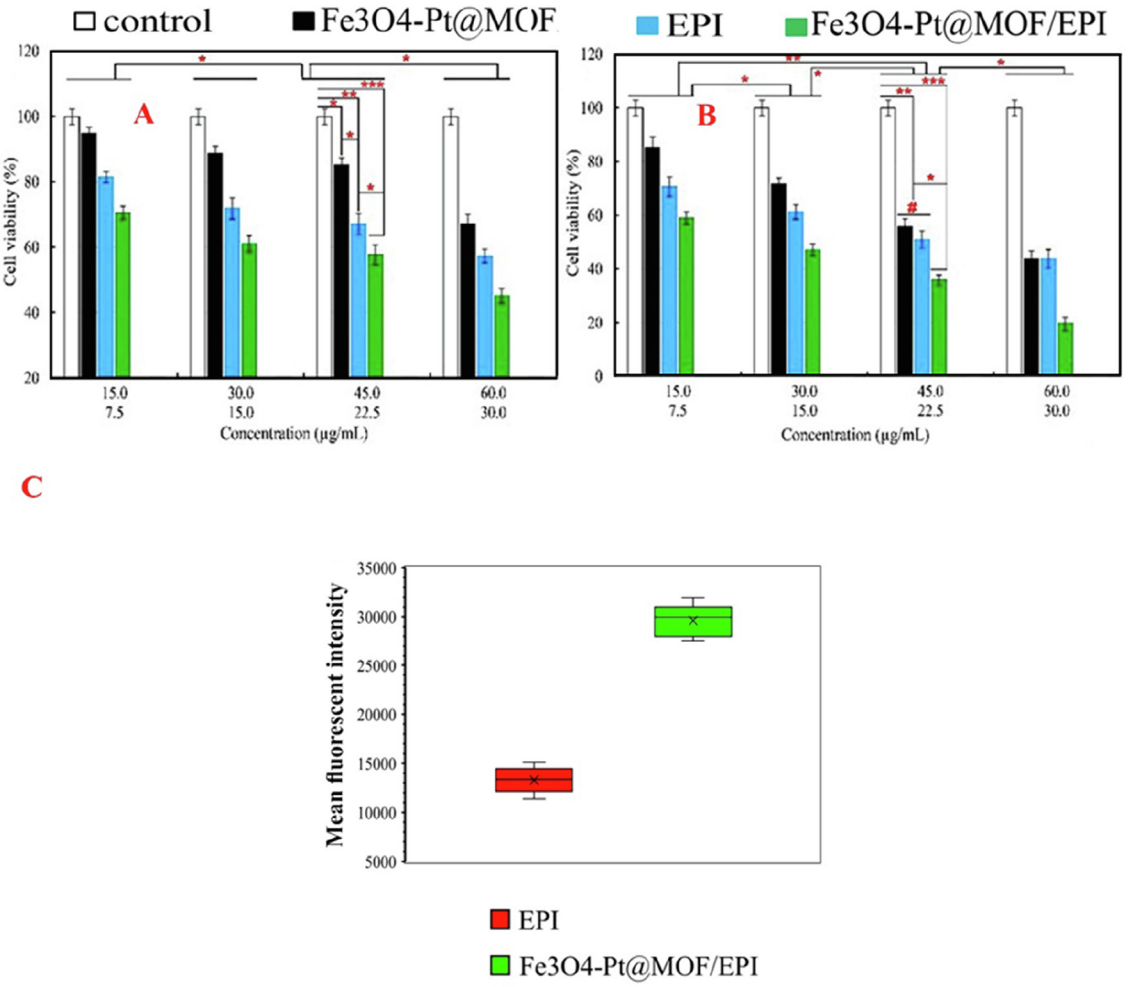

Fig. 4. Viability assay of NIH3T3 (A) and triple-negative 4 T1 breast (TNFB) cancer cells (B) treated with EPI (Epirubicin), Fe_3O_4-Pt, core–shell Fe_3O_4-Pt@MOF nanospheres, and core–shell Fe_3O_4-Pt@MOF/EPI nanospheres (C) mean fluorescent intensity in TNFB cancer cells cultured with EPI, and core–shell Fe_3O_4-Pt@MOF/EPI nanospheres. $^{*}P < 0.05$, $^{**}P < 0.01$ and $^{***}P < 0.001$ for a difference of treated groups.

(2015), changing the pH of the environment causes the breakdown of the coating and the release of the drug in acidic environments, high accumulation of EPI in TNFB tumor with a mildly acidic pH is expected.

3.3. Cytotoxicity assay and cell penetrating

Fig. 4A and 4B show that, while increased EPI and nanospheres concentrations in both NIH3T3 and TNFB cancer cells cause significant toxicity, the toxic effects of EPI and nanospheres concentrations on TNFB cancer cells are nearly two-fold higher than that of NIH3T3 cells. The highest toxicity of nanospheres and EPI against TNFB cancer cells was determined to be 60 μg/mL and 30 μg/mL, respectively (Fig. 4B). Furthermore, while the toxicity of core–shell Fe_3O_4-Pt@MOF nanospheres and EPI-treated groups were comparable in NIH3T3 cells and, to a lesser extent, TNFB cancer cells, the drug-loaded core–shell Fe_3O_4-Pt@MOF/EPI nanospheres induce higher toxicity than EPI in both cell lines, particularly TNFB cancer cells.

Besides that, the results of Fig. 4A and 4B show that NIH3T3 cells are more biocompatible than TNFB cancer cells against Fe_3O_4 nanospheres, especially at concentrations of 15 and 30 μg/mL, with 94.9 % and 88.7 % viability, respectively. Moreover, the survival rate of TNFB cancer cells following exposure to core–shell Fe_3O_4-Pt@MOF/EPI nanospheres at concentrations of 15, 30, 45, and 60 g/mL reduced to 58.9, 47.1, 35.9, and 19.6 %, respectively. Overall, the results show that core–shell Fe_3O_4-Pt@MOF/EPI nanospheres have a high anticancer efficacy in TNFB cancer cells.

The fluorescence output in Fig. 4C confirms this finding by demonstrating that the use of the core–shell Fe_3O_4-Pt@MOF/EPI nanospheres in comparison to free EPI effectively increases the internalization of EPI in TNFB cancer cells based on the enhancement of fluorescence intensity in the TNFB cancer cells.

At low concentrations, EPI is an antitumor drug with low efficacy (Fogarassy, Vathy-Fogarassy et al. 2019). Long-term use of EPI at high concentrations is recommended to increase its effectiveness, but this can cause significant toxicity in the brain, bone marrow (aplasia), liver, kidney, gastrointestinal tract (bleeding), and other organs (Coukell and Faulds 1997). Several promising nanocarriers for delivering EPI to tumor sites have been reported in recent years (Chen, Han et al. 2019, De Vita, Liverani et al. 2021, Leng, Li et al. 2021, Seki, Higeta et al. 2021). The loading efficiency of EPI on nanoparticles, however, is limited. The use of core (metal oxide nanoparticles)-shell (chemical compounds) nanospheres with controllable multiple behavioral properties due to high drug loading capacity, reduced toxicity, reduced agglomeration, targeting, and the possibility of auxiliary cancer therapeutic is critical in this regard (Chien, Cheng et al. 2021, Pooresmaeil, Asl et al. 2021, Sun, He et al. 2021). In this study, the hydrothermal and layer-by-layer methods were used to create the core–shell Fe_3O_4-Pt@MOF/EPI nanospheres, similar to the studies of Ebrahimi, Barani et al. (2018) and Chen, Zhang et al. (2019). Despite the difficulty of targeting and controlling drug release, the multi-stage or layer-by-layer manufacturing process is reliable (Aghayi-Anaraki and Safarifard 2020, Szczęch and Szczepanowicz 2020).

The observed dose-dependent toxicity of the core–shell Fe_3O_4-Pt@MOF/EPI nanospheres against TNFB cancer cells is consistent with the findings of Chowdhuri, Bhattacharya et al. (2016) and Pooresmaeil, Asl et al. (2021) results.

4. Conclusions

In general, Fe_3O_4-Pt@MOF nanospheres with a core–shell structure containing EPI was synthesized by hydrothermal and layer-by-layer methods. The results of SEM, TGA, DLS, N_2 adsorption, and XRD analyses confirmed a spherical shape of nanospheres with high porosity on which MOF and EPI are loaded. In addition, a selective anticancer effect against TNFB cancer cells was observed due to higher cellular uptake of EPI in the form of nanoformulation than that of free form. A major limitation of this paper can be evaluating the anticancer effects of developed Fe_3O_4-Pt@MOF/EPI nanoplatform *in vitro*, which does not reflect the inherent complexity of organ systems. Therefore, further *in vivo* and preclinical studies are required to be done in future studies to validate the data presented in this study.

Funding

This study was supported by the Project of Ningbo Science and Technology Bureau (NO.2019B10039), Project of Ningbo Clinical Research Center for Thoracic & Breast Neoplams (NO. 2021L002), and Project of Ningbo Medical & Health Leading Academic Discipline (NO. 2022-F03).

CRediT authorship contribution statement

Jiadi Li: Conceptualization, Investigation, Methodology, Writing – original draft, Writing – review & editing, Formal analysis, Visualization. **Yuxin Zhou:** Conceptualization, Investigation, Methodology, Writing – original draft, Writing – review & editing, Formal analysis, Visualization. **Shuixin Yan:** Conceptualization, Investigation, Methodology, Writing – original draft, Writing – review & editing, Formal analysis, Visualization. **Weizhu Wu:** Conceptualization, Investigation, Methodology, Writing – original draft, Writing – review & editing, Formal analysis, Visualization. **Majid Sharifi:** Conceptualization, Investigation, Methodology, Writing – original draft, Writing – review & editing, Formal analysis, Visualization.

Declaration of Competing Interest

The authors declare that they have no known competing financial interests or personal relationships that could have appeared to influence the work reported in this paper.

References

Aghayi-Anaraki, M., Safarifard, V., 2020. Fe3O4@MOF magnetic nanocomposites: Synthesis and applications. Eur. J. Inorg. Chem. 2020 (20), 1916–1937.

Alijani, H., Noori, A., Faridi, N., Bathaie, S.Z., Mousavi, M.F., 2020. Aptamer-functionalized Fe3O4@ MOF nanocarrier for targeted drug delivery and fluorescence imaging of the triple-negative MDA-MB-231 breast cancer cells. J. Solid State Chem. 292, 121680.

Bag, P.P., Wang, D., Chen, Z., Cao, R., 2016. Outstanding drug loading capacity by water stable microporous MOF: a potential drug carrier. Chem. Commun. 52 (18), 3669–3672.

Chen, X., Han, W., Zhao, X., Tang, W., Wang, F., 2019. Epirubicin-loaded marine carrageenan oligosaccharide capped gold nanoparticle system for pH-triggered anticancer drug release. Sci. Rep. 9 (1), 6754.

Chen, J., Liu, J., Hu, Y., Tian, Z., Zhu, Y., 2019. Metal-organic framework-coated magnetite nanoparticles for synergistic magnetic hyperthermia and chemotherapy with pH-triggered drug release. Sci. Technol. Adv. Mater. 20 (1), 1043–1054.

Chen, X., Zhang, Y., Zhao, Y., Wang, S., Liu, L., Xu, W., Guo, Z., Wang, S., Liu, Y., Zhang, J., 2019. Encapsulating Pt nanoparticles through transforming Fe3O4 into MIL-100(Fe) for well-defined Fe3O4@Pt@MIL-100(Fe) core-shell heterostructures with promoting catalytic activity. Inorg. Chem. 58 (18), 12433–12440.

Chien, W.-C., P.-H. Cheng, X.-J. Cheng, C.-C. Chuang, Y.-T. Huang, A. TS, C.-H. Liu, Y.-J. Lu and K. C.-W. Wu (2021). "MCP-1-Functionalized, Core–Shell Gold Nanorod@ Iron-Based Metal–Organic Framework (MCP-1/GNR@ MIL-100 (Fe)) for Photothermal Therapy." ACS Applied Materials & Interfaces.

Chowdhuri, A.R., Bhattacharya, D., Sahu, S.K., 2016. Magnetic nanoscale metal organic frameworks for potential targeted anticancer drug delivery, imaging and as an MRI contrast agent. Dalton Trans. 45 (7), 2963–2973.

Coukell, A.J., Faulds, D., 1997. Epirubicin. Drugs 53 (3), 453–482.

Cui, R., Zhao, P., Yan, Y., Bao, G., Damirin, A., Liu, Z., 2021. Outstanding drug-loading/release capacity of hollow Fe-metal–organic framework-based microcapsules: A potential multifunctional drug-delivery platform. Inorg. Chem. 60 (3), 1664–1671.

da Silva, J.L., Nunes, N.C.C., Izetti, P., de Mesquita, G.G., de Melo, A.C., 2020. Triple negative breast cancer: A thorough review of biomarkers. Crit. Rev. Oncol. Hematol. 145, 102855.

De Vita, A., Liverani, C., Molinaro, R., Martinez, J.O., Hartman, K.A., Spadazzi, C., Miserocchi, G., Taraballi, F., Evangelopoulos, M., Pieri, F., Bongiovanni, A., Mercatali, L., Tasciotti, E., Ibrahim, T., 2021. Lysyl oxidase engineered lipid nanovesicles for the treatment of triple negative breast cancer. Sci. Rep. 11 (1), 5107.

Desoize, B., Madoulet, C., 2002. Particular aspects of platinum compounds used at present in cancer treatment. Crit. Rev. Oncol. Hematol. 42 (3), 317–325.

DİNÇER, C. A., B. GETİREN, C. GÖKALP, Z. ÇIPLAK, A. KARAKEÇİLİ and N. YILDIZ (2021). "An anticancer drug loading and release study to ternary GO-Fe3O4-PPy and Fe3O4@ PPy-NGQDs nanocomposites for photothermal chemotherapy." Colloids and Surfaces A: Physicochemical and Engineering Aspects: 127791.

Ebrahimi, A.K., Barani, M., Sheikhshoaie, I., 2018. Fabrication of a new superparamagnetic metal-organic framework with core-shell nanocomposite structures: Characterization, biocompatibility, and drug release study. Mater. Sci. Eng. C 92, 349–355.

Falahati, M., Sharifi, M., Ten Hagen, T.L., 2022. Explaining chemical clues of metal organic framework-nanozyme nano-/micro-motors in targeted treatment of cancers: benchmarks and challenges. J. Nanobiotechnol. 20 (1), 1–26.

Fathian kolahkaj, F., K. Derakhshandeh, F. Khaleseh, A. H. Azandaryani, K. Mansouri and M. Khazaei (2019). "Active targeting carrier for breast cancer treatment: Monoclonal antibody conjugated epirubicin loaded nanoparticle." Journal of Drug Delivery Science and Technology **53**: 101136.

Fogarassy, G., Vathy-Fogarassy, Á., Kenessey, I., Kásler, M., Forster, T., 2019. Risk prediction model for long-term heart failure incidence after epirubicin chemotherapy for breast cancer–a real-world data-based, nationwide classification analysis. Int. J. Cardiol. 285, 47–52.

Jain, V., Kumar, H., Anod, H.V., Chand, P., Gupta, N.V., Dey, S., Kesharwani, S.S., 2020. A review of nanotechnology-based approaches for breast cancer and triple-negative breast cancer. J. Control. Release 326, 628–647.

Jalalian, S.H., Ramezani, M., Abnous, K., Taghdisi, S.M., 2018. Targeted co-delivery of epirubicin and NAS-24 aptamer to cancer cells using selenium nanoparticles for enhancing tumor response in vitro and in vivo. Cancer Lett. 416, 87–93.

Ke, F., Qiu, L.-G., Yuan, Y.-P., Jiang, X., Zhu, J.-F., 2012. Fe 3 O 4@ MOF core–shell magnetic microspheres with a designable metal–organic framework shell. J. Mater. Chem. 22 (19), 9497–9500.

Khan, S., Sharifi, M., Hasan, A., Attar, F., Edis, Z., Bai, Q., Derakhshankhah, H., Falahati, M., 2021. Magnetic nanocatalysts as multifunctional platforms in cancer therapy through the synthesis of anticancer drugs and facilitated Fenton reaction. J. Adv. Res. 30, 171–184.

Khasraw, M., Bell, R., Dang, C., 2012. Epirubicin: Is it like doxorubicin in breast cancer? A clinical review. Breast 21 (2), 142–149.

Klein, S., J. Otto, C. Harreiß, L. V. Distel, A. Leistner, W. Neuhuber, E. Spiecker and C. Kryschi (2021). "Pt–Fe3O4, Pd–Fe3O4, and Au–Fe3O4 Nanoheterodimers and Their Efficacy as Radiosensitizers in Cancer Therapy." ACS Applied Bio Materials.

Leng, Q., Li, Y., Zhou, P., Xiong, K., Lu, Y., Cui, Y., Wang, B., Wu, Z., Zhao, L., Fu, S., 2021. Injectable hydrogel loaded with paclitaxel and epirubicin to prevent postoperative recurrence and metastasis of breast cancer. Mater. Sci. Eng. C 129, 112390.

Marra, A., Trapani, D., Viale, G., Criscitiello, C., Curigliano, G., 2020. Practical classification of triple-negative breast cancer: intratumoral heterogeneity, mechanisms of drug resistance, and novel therapies. npj Breast Cancer 6 (1), 1–16.

Meng, F., Zhang, S., Ma, L., Zhang, W., Li, M., Wu, T., Li, H., Zhang, T., Lu, X., Huo, F., 2018. Construction of hierarchically porous nanoparticles@ metal–organic frameworks composites by inherent defects for the enhancement of catalytic efficiency. Adv. Mater. 30 (49), 1803263.

Moammeri, A., Abbaspour, K., Zafarian, A., Jamshidifar, E., Motasadizadeh, H., Dabbagh Moghaddam, F., Salehi, Z., Makvandi, P., Dinarvand, R., 2022. pH-responsive, adorned nanoniosomes for codelivery of cisplatin and epirubicin: Synergistic treatment of breast cancer. ACS Appl. Bio Mater. 5 (2), 675–690.

Plosker, G.L., Faulds, D., 1993. Epirubicin. Drugs 45 (5), 788–856.

Pooresmaeil, M., Asl, E.A., Namazi, H., 2021. A new pH-sensitive CS/Zn-MOF@ GO ternary hybrid compound as a biofriendly and implantable platform for prolonged 5-Fluorouracil delivery to human breast cancer cells. J. Alloy. Compd. 885, 160992.

Qi, Y., Ye, J., Ren, S., Lv, J., Zhang, S., Che, Y., Ning, G., 2020. In-situ synthesis of metal nanoparticles@ metal– organic frameworks: Highly effective catalytic performance and synergistic antimicrobial activity. J. Hazard. Mater. 387, 121687.

Rao, Y.-F., Chen, W., Liang, X.-G., Huang, Y.-Z., Miao, J., Liu, L., Lou, Y., Zhang, X.-G., Wang, B., Tang, R.-K., Chen, Z., Lu, X.-Y., 2015. Epirubicin-loaded superparamagnetic iron-oxide nanoparticles for transdermal delivery: Cancer therapy by circumventing the skin barrier. Small 11 (2), 239–247.

Rottenberg, S., Disler, C., Perego, P., 2021. The rediscovery of platinum-based cancer therapy. Nat. Rev. Cancer 21 (1), 37–50.

Seki, H., Higeta, K., Sakurai, T., Sakurada, A., Kinoshita, T., Shimizu, K., 2021. Feasibility study of nanoparticle albumin-bound-paclitaxel and S-1 followed by epirubicin/cyclophosphamide as neoadjuvant chemotherapy in patients with operable breast cancer: A prospective study. Clin. Breast Cancer.

Sharifi, M., Hosseinali, S.H., Saboury, A.A., Szegezdi, E., Falahati, M., 2019. Involvement of planned cell death of necroptosis in cancer treatment by nanomaterials: Recent advances and future perspectives. J. Control. Release 299, 121–137.

Sharifi, M., Jafari, S., Hasan, A., Paray, B.A., Gong, G., Zheng, Y., Falahati, M., 2020. Antimetastatic activity of lactoferrin-coated mesoporous maghemite nanoparticles in breast cancer enabled by combination therapy. ACS Biomater. Sci. Eng. 6 (6), 3574–3584.

Sharifi, M., Hasan, A., Nanakali, N.M.Q., Salihi, A., Qadir, F.A., Muhammad, H.A., Shekha, M.S., Aziz, F.M., Amen, K.M., Najafi, F., Yousefi-Manesh, H., Falahati, M., 2020. Combined chemo-magnetic field-photothermal breast cancer therapy based on porous magnetite nanospheres. Sci. Rep. 10 (1), 5925.

Sun, X., He, G., Xiong, C., Wang, C., Lian, X., Hu, L., Li, Z., Dalgarno, S.J., Yang, Y.-W., Tian, J., 2021. One-pot fabrication of hollow porphyrinic MOF nanoparticles with ultrahigh drug loading toward controlled delivery and synergistic cancer therapy. ACS Appl. Mater. Interfaces 13 (3), 3679–3693.

Szczęch, M., Szczepanowicz, K., 2020. Polymeric core-shell nanoparticles prepared by spontaneous emulsification solvent evaporation and functionalized by the layer-by-layer method. Nanomaterials (Basel, Switzerland) 10 (3), 496.

Tang, H., Chen, J., Wang, L., Li, Q., Yang, Y., Lv, Z., Bao, H., Li, Y., Luan, X., Li, Y., Ren, Z., Zhou, X., Cong, D., Liu, Z., Jia, J., Chen, H., Zhao, W., Meng, Q., Sun, F., Pei, J., 2020. Co-delivery of epirubicin and paclitaxel using an estrone-targeted PEGylated liposomal nanoparticle for breast cancer. Int. J. Pharm. 573, 118806.

Wang, C., DeKrafft, K.E., Lin, W., 2012. Pt nanoparticles@ photoactive metal–organic frameworks: efficient hydrogen evolution via synergistic photoexcitation and electron injection. J. Am. Chem. Soc. 134 (17), 7211–7214.

Wang, Z., Yu, W., Yu, N., Li, X., Feng, Y., Geng, P., Wen, M., Li, M., Zhang, H., Chen, Z., 2020. Construction of CuS@ Fe-MOF nanoplatforms for MRI-guided synergistic photothermal-chemo therapy of tumors. Chem. Eng. J. 400, 125877.

Wu, M.X., Gao, J., Wang, F., Yang, J., Song, N., Jin, X., Mi, P., Tian, J., Luo, J., Liang, F., 2018. Multistimuli responsive core–shell nanoplatform constructed from Fe3O4@ MOF equipped with pillar [6] arene nanovalves. Small 14 (17), 1704440.

Xiang, Z., Qi, Y., Lu, Y., Hu, Z., Wang, X., Jia, W., Hu, J., Ji, J., Lu, W., 2020. MOF-derived novel porous Fe 3 O 4@ C nanocomposites as smart nanomedical platforms for combined cancer therapy: magnetic-triggered synergistic hyperthermia and chemotherapy. J. Mater. Chem. B 8 (37), 8671–8683.

Yamaguchi, N., Fujii, T., Aoi, S., Kozuch, P.S., Hortobagyi, G.N., Blum, R.H., 2015. Comparison of cardiac events associated with liposomal doxorubicin, epirubicin and doxorubicin in breast cancer: a Bayesian network meta-analysis. Eur. J. Cancer 51 (16), 2314–2320.

Yang, Y., Xia, F., Yang, Y., Gong, B., Xie, A., Shen, Y., Zhu, M., 2017. Litchi-like Fe 3 O 4@ Fe-MOF capped with HAp gatekeepers for pH-triggered drug release and anticancer effect. J. Mater. Chem. B 5 (43), 8600–8606.

Yang, Y., Zeng, Z., Almatrafi, E., Huang, D., Zhang, C., Xiong, W., Cheng, M., Zhou, C., Wang, W., Song, B., 2022. Core-shell structured nanoparticles for photodynamic therapy-based cancer treatment and related imaging. Coord. Chem. Rev. 458, 214427.

Yue, L., Cao, Y., Han, Y., Li, Z., Luo, X., Liu, Y., 2021. Preparation of core-shell structured Fe3O4@ Sn-MOF composite and photocatalytic performance. J. Alloy. Compd. 870, 159339.

Zhao, J., M. Li, J. Duan, H. Guo and D. Yu (2021). "Multifunctional PD-L1 Targeted Fe3O4@ DOX Nanoparticles Under MRI Monitoring For Combination Therapy of Triple-Negative Breast Cancer.".